PERGAMON

Engineering Fracture Mechanics 67 (2000) 209–227

Engineering Fracture Mechanics

www.elsevier.com/locate/engfracmech

Mixed-mode, high-cycle fatigue-crack growth thresholds in Ti–6Al–4V
I. A comparison of large- and short-crack behavior

J.P. Campbell, R.O. Ritchie *

Department of Materials Science and Mineral Engineering, University of California, 463 Evans Hall, Berkeley, CA 94720-1760, USA

Received 27 December 1999; received in revised form 4 May 2000; accepted 11 May 2000

Abstract

Mixed-mode, high-cycle fatigue-crack growth thresholds are reported for through-thickness cracks (large compared to microstructural dimensions) in a Ti–6Al–4V turbine blade alloy with a bimodal microstructure. Specifically, the effect of combined mode I and mode II loading, over a range of phase angles $\beta = \tan^{-1}(\Delta K_{II}/\Delta K_I)$ from 0° to 82° ($\Delta K_{II}/\Delta K_I \sim 0$–7), is examined for load ratios (ratio of minimum to maximum loads) ranging from $R = 0.1$ to 0.8 at a cyclic loading frequency of 1000 Hz in ambient temperature air. Although the general trend for the mode I stress-intensity range at the threshold, $\Delta K_{I,TH}$, is to decrease with increasing mode mixity, $\Delta K_{II}/\Delta K_I$, and load ratio, R, if the crack-driving force is alternatively characterized in terms of the strain-energy release rate, ΔG, incorporating contributions from both the applied tensile and shear loading, the threshold fatigue-crack growth resistance increases significantly with the applied ratio of $\Delta K_{II}/\Delta K_I$. The pure mode I threshold, in terms of ΔG_{TH}, is observed to be a lower bound (worst case) with respect to mixed-mode (I + II) behavior. These results are compared with mixed-mode fatigue thresholds for short cracks, where the precrack wake has been machined to within ~200 μm of the precrack tip. For such short cracks, wherein the magnitude of crack-tip shielding which can develop is greatly reduced, the measured mixed-mode fatigue-crack growth thresholds are observed to be markedly lower. Moreover, the dependence of the mixed-mode fatigue-crack growth resistance on the applied phase angle is significantly reduced. Comparison of the large- and short-crack data suggests that the increase in the large-crack fatigue threshold, ΔG_{TH}, with an increasing mode mixity ($\Delta K_{II}/\Delta K_I$) is largely due to shielding from shear-induced crack-surface contact, which reduces the local crack-driving force actually experienced at the crack tip. Quantification of such shielding is described in Part II of this paper.

Keywords: High-cycle fatigue; Mixed mode; Fatigue thresholds; Load ratio effects; Short crack effects; Crack-tip shielding

* Corresponding author. Tel.: +510-486-5798; fax: +510-486-4995.
E-mail address: roritchie@lbl.gov (R.O. Ritchie).

0013-7944/00/$ - see front matter
PII: S0013-7944(00)00046-1

1. Introduction

One of the principal challenges currently associated with the safety and readiness of military aircraft fleets is the susceptibility of turbine engine components to failure from high-cycle fatigue (HCF), i.e., the rapid propagation of fatigue cracks under high frequency vibratory loading [1,2]. Such failures are extremely costly, leading to severe engine damage, loss of aircraft, and even loss of human life. Multiaxial loading conditions are known to exist at specific fatigue-critical locations within the turbine engine components, particularly in association with fretting fatigue in the blade dovetail/disk contact section [3]. For fatigue-crack growth in such situations, the resultant crack-driving force may be a combination of the influence of a mode I (tensile opening) stress-intensity range, ΔK_I, as well as mode II (in-plane shear) and/or mode III (anti-plane shear) stress-intensity ranges, ΔK_{II} and ΔK_{III}, respectively. While the vast majority of the published fatigue-crack growth data is measured for mode I loading only, it has been observed that the superposition of cyclic shear (ΔK_{II} or $\Delta K_{III} > 0$) to cyclic tension can lower the mode I threshold stress-intensity range, ΔK_I, below which crack growth is presumed dormant [4–12]. Recent studies in single crystal Ni-based superalloys show that this effect can be severe [13].

For the high-cycle fatigue of turbine engine alloys, it is clearly critical to quantify the effect of combined tension and shear loading on the fatigue-crack growth threshold, as the extremely high cyclic loading frequencies (~1–2 kHz) and correspondingly short times to failure may necessitate a threshold-based design methodology [14]. Given this, as well as the knowledge of the existence of such loading conditions in fatigue-critical components, the paucity of mixed-mode fatigue-crack propagation data in aerospace titanium alloys [5–7] is of some concern. Of further concern is the almost total lack of information on mixed-mode thresholds for cracks of limited dimensions, i.e., compared to the scale of microstructure or extent of crack-tip shielding; extensive results for behavior under nominal mode I loading indicate that the fatigue thresholds for the so-called small or short cracks can be significantly smaller than those measured for corresponding large cracks [15–22]. [1]

Accordingly, in the present work, mixed-mode fatigue-crack growth thresholds for combined mode I + II loading are examined in a Ti–6Al–4V alloy with a typical turbine blade microstructure. The influence of various degrees of mode-mixity, ranging from $\Delta K_{II}/\Delta K_I = 0$ (mode I loading) to ~7, on the crack-growth threshold condition is investigated for loading conditions characteristic of turbine engine HCF, i.e. high mean stresses (up to load ratios of $R = 0.8$) and high cyclic loading frequencies (1000 Hz). Experiments are performed using an asymmetric bend geometry for both large (>4 mm) and short (~150–250 μm) cracks; the latter is achieved by machining out the wake of larger cracks to within ~200 μm of the crack tip. Since both types of flaws are through thickness (~5 mm) and large compared to microstructural size scales (i.e., the grain size) in this dimension, in both cases, their crack fronts are able to "sample" many microstructural entities; such flaws may be termed "continuum-sized" cracks. However, the capacity for crack-tip shielding is significantly reduced with the short crack due to the restricted crack wake in which fracture surface contact mechanisms can operate.

It is found that, although the value of the mode I stress-intensity range at threshold, $\Delta K_{I,TH}$, can be *decreased* for a sufficiently high ratio $\Delta K_{II}/\Delta K_I$, provided the mixed-mode crack-driving force is characterized in terms of the strain-energy release rate, ΔG_{TH}, (incorporating both tensile and shear contributions), the (large-crack) fatigue-crack growth threshold actually *increases* with increasing mode-mixity. Thus, the mode I fatigue-crack growth threshold, *expressed in terms of* ΔG_{TH}, is the worst-case (at least for continuum-sized cracks). This strong dependence of ΔG_{TH} on mode mixity is found to be reduced for short cracks, primarily due to a reduced role of crack-tip shielding; moreover, the magnitude of the ΔG_{TH}

[1] A brief description of the salient distinctions between large, short and small fatigue cracks can be found in Appendix A.

threshold for such short cracks is found to be lower than that exhibited by the large cracks for all values of $\Delta K_{II}/\Delta K_I$ studied.

2. Materials and experimental methods

2.1. Material

The material investigated was a forged Ti–6Al–4V turbine engine alloy received with a bimodal microstructure [2] consisting of nearly equiaxed primary α and lamellar α + β colonies (Fig. 1). This alloy was processed specifically for the joint military–industry–university HCF program by Teledyne Titanium as mill-annealed, forging bar-stock material (diameter: 63.5 mm); its chemical composition is given in Table 1. The β-transus temperature, measured using differential thermal analysis, ranged from 990°C to 1005°C.

The bar stock was sectioned into 400 mm long segments, preheated to 940°C (30 min), and forged into $400 \times 150 \times 20$ mm^3 plates. The forged plates were then solution treated at 925°C (1 h) in air, followed by fan air cooling, and a subsequent stabilization was performed at 700°C (2 h) in vacuo. Based on the measurements in each of the four random forging locations [24], the microstructure was found to consist of 64.1 vol.% (standard deviation: 6.6%) primary α with an average grain diameter of ~20 μm (slightly elongated in the longitudinal (L) direction) and lamellar α + β colonies (Fig. 1); the lamellar spacing (center-to-center

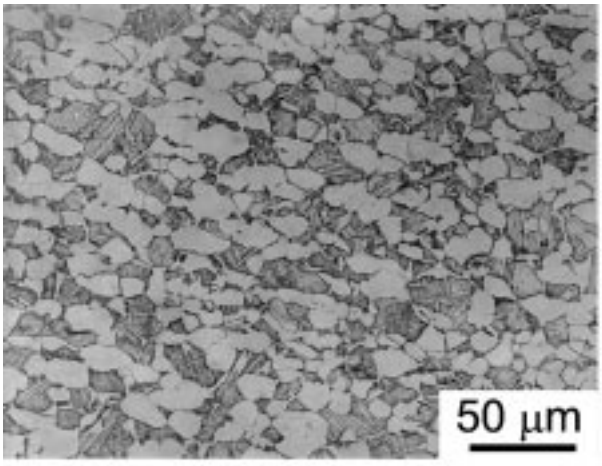

Fig. 1. Optical photomicrograph of the bimodal (STOA) Ti–6Al–4V. The bimodal structure consists of nearly equiaxed grains of primary α phase (~20 μm in diameter) and regions of lamellar α + β. Etchant: aqueous 3.5% HNO_3, and 5% HF.

Table 1
Chemical composition of Ti–6Al–4V bar stock (in wt.%) [23]

Bar location	Ti	Al	V	Fe	O	N	H
Top	Balance	6.27	4.19	0.20	0.18	0.012	0.0041
Bottom	Balance	6.32	4.15	0.18	0.19	0.014	0.0041

[2] This microstructural condition is often referred to as solution treated and overaged (STOA) by the HCF community.

distance for the β phase) was measured from phase contrast (backscattered electron imaging) scanning electron micrographs to be ~1 μm.

Tensile tests, conducted at initial strain rates of 5×10^{-4} s^{-1} in the longitudinal (L) orientation [23], indicated a yield strength of 930 MPa (range: 926–935 MPa) and an ultimate tensile strength of 978 MPa (range: 970–985 MPa).

2.2. Experimental methods

Thresholds for large fatigue cracks were measured using the asymmetric four-point bend (AFPB) specimen [4,25–27]. For this test geometry, the bending moment, M_z, varies linearly between the inner loading points, while the shear force, F_{xy}, is constant in this region (Fig. 2). Thus, a cracked sample may be subjected to loading conditions ranging from pure mode II to mode I dominant (i.e., a small value of $\Delta K_{II}/\Delta K_I$) by careful control of the distance by which the crack is offset from the load line, s. Pure mode I tests were conducted using standard, symmetric four-point bend. Inner and outer loading spans (from load line to loading point) of 12.7 and 25.4 mm, respectively, were utilized. A high pressure MoS_2 grease was applied at the loading points to minimize the effects of friction. Mixed-mode loading conditions were quantified both in terms of the ratio of $\Delta K_{II}/\Delta K_I$, which was varied from 0 (pure mode I) to 7.1, and the phase angle, $\beta = \tan^{-1}(\Delta K_{II}/\Delta K_I)$, which correspondingly varied from 0° to 82°. Positive load ratios ($R = K_{min}/K_{max}$) were varied between 0.1 and 0.8.

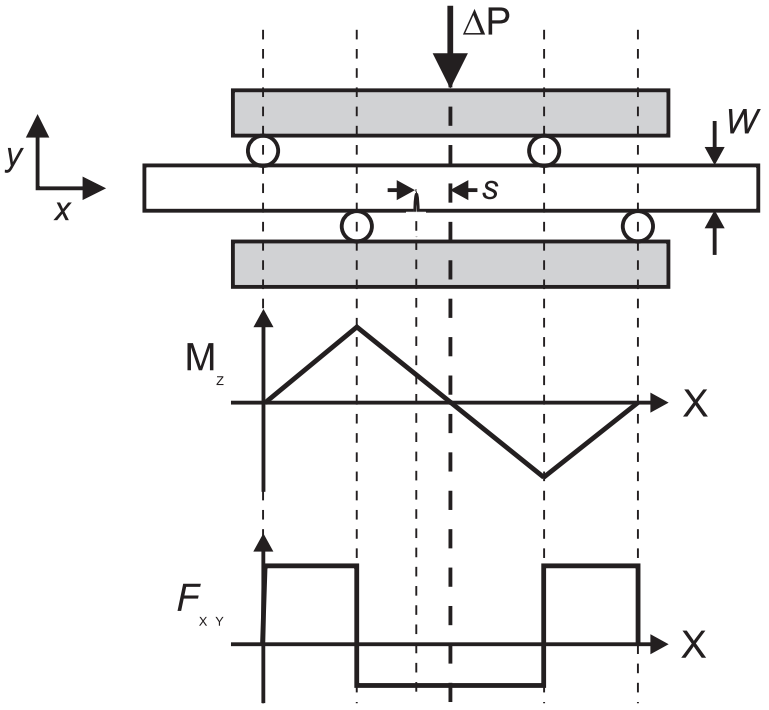

Fig. 2. The asymmetric, four-point-bend, crack-growth sample and the associated shear force, F_{xy}, and bending moment, M_z, diagrams are shown. When the crack is offset from the load line by an amount s, the value of s/W (where W is the beam height) dictates the ratio of ΔK_{II} to ΔK_I.

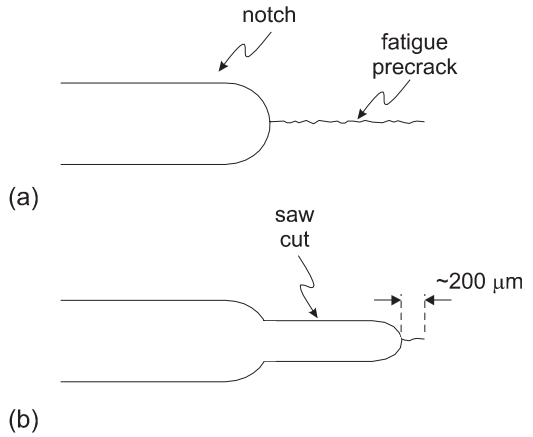

Fig. 3. The first step of fatigue precracking for short-crack threshold measurements was conducted in the same manner as for large-crack threshold measurements, as shown in (a). Following this procedure, the precrack wake was machined out using a slow speed diamond saw (b) to within ~200 μm of the precrack tip. Mixed-mode thresholds for short fatigue cracks were then measured by the same methods employed for large fatigue cracks.

Because of the potentially strong influence on mixed-mode crack-growth behavior of precracking technique [9] and crack-wake shielding effects [4,28–31], a very specific fatigue precracking regimen was employed to ensure a standard and reproducible precrack condition for all the threshold measurements. Fatigue precracks were grown, using computer-automated stress-intensity control, from a 2 mm deep electrical discharge machined notch under mode I loading in four-point bending, with a load ratio, $R = K_{\min}/K_{\max}$, of 0.1, and a cyclic loading frequency of 125 Hz (sine wave). Loads were shed at a K-gradient, [3] C, of -0.15 mm^{-1} such that a final precrack length of 4.50 ± 0.25 mm was achieved at a near threshold stress intensity range of 4.8 ± 0.3 MPa $\sqrt{}$m.

To determine fatigue thresholds, tests were performed on an MTS servo-hydraulic high-frequency testing machine incorporating a voice-coil servovalve [32]. AFPB samples were loaded with the precrack tip offset from the load line to achieve the desired ratio $\Delta K_{II}/\Delta K_I$. The necessary offset and values of ΔK_I and ΔK_{II} corresponding to the applied load amplitude were determined using a recently updated stress-intensity solution for the AFPB geometry by He and Hutchinson [26]. Samples were then subjected to two million cycles at 1000 Hz (sine wave). If no crack growth was observed (via an optical microscope), ΔK_I or ΔK_{II} was increased by approximately 0.25 MPa $\sqrt{}$m and the test was repeated. In this way, the threshold for the onset of crack growth (defined as crack growth rates less than 10^{-11} m/cycle) was measured as a "growth/no growth" set of loading conditions bounding the true threshold.

Fatigue precracks for short-crack threshold measurements were generated as described above. Following this procedure, the precrack wake was machined out using a slow speed diamond saw to within ~200 μm of the precrack tip, as illustrated in Fig. 3. This technique significantly restricts the degree of crack wake contact during subsequent mixed-mode loading and, hence, markedly reduces the magnitude of crack-tip shielding. Mixed-mode fatigue-crack growth thresholds were then measured by the same methods employed for large fatigue cracks.

[3] The K-gradient, C, is defined by the equation $\Delta K_0 = \Delta K_i \exp(C(a_0 - a_i))$, where subscripts "0" and "i" indicate current and initial parameter values.

3. Results and discussion

3.1. Mixed-mode threshold envelopes

Mixed-mode fatigue-crack growth threshold envelopes, plotted as the mode II stress-intensity range at threshold, $\Delta K_{II,TH}$, as a function of the corresponding mode I threshold, $\Delta K_{I,TH}$, are shown in Fig. 4. The thresholds for the onset of crack extension are presented for $\Delta K_{II}/\Delta K_{I}$ values of 0, 0.5, 1.9 and 7.1 ($\beta = 0°$, 26°, 62° and 82°, respectively) at load ratios of 0.1, 0.5 and 0.8. Closed and open symbols represent the loading conditions that produced, respectively, no crack growth and crack growth; these loading conditions bound the true threshold for the onset of crack extension. An error analysis for these threshold data is presented in Appendix B; uncertainty in the position of the crack with respect to the mechanical test frame load line and the associated uncertainty in $\Delta K_{I,TH}$ and the applied phase angle are considered.

Comparison of the three load ratios investigated reveals that the fatigue-crack growth resistance is degraded by increasing R, as evidenced by a shifting of the threshold envelope towards lower values of $\Delta K_{I,TH}$ and $\Delta K_{II,TH}$. These findings are consistent with the previous reports regarding the influence of load ratio on mixed-mode fatigue-crack growth thresholds in other material systems [4,10]. Further discussion of the influence of load ratio on mixed-mode thresholds is presented below.

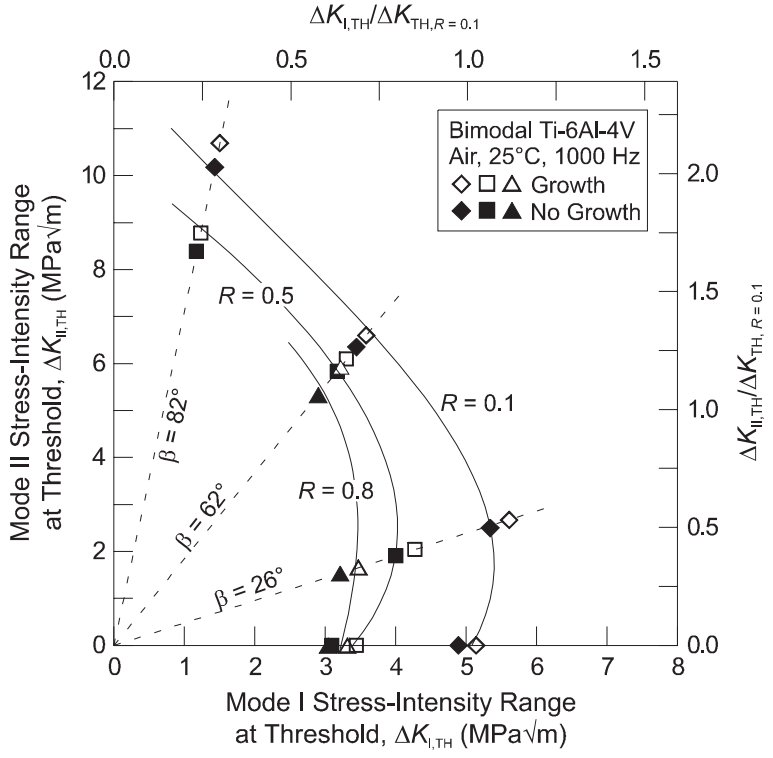

Fig. 4. Mixed-mode fatigue-crack growth threshold envelopes for bimodal Ti–6Al–4V at load ratios, R, of 0.1, 0.5 and 0.8 and a cyclic loading frequency of 1000 Hz in ambient temperature air. Closed and open symbols represent the loading conditions that produced, respectively, no crack growth and crack growth; these loading conditions bound the true threshold for the onset of crack extension. On the upper and right-hand axes, $\Delta K_{I,TH}$ and $\Delta K_{II,TH}$ are normalized by the pure mode I threshold at $R = 0.1$, $\Delta K_{TH,R=0.1}$.

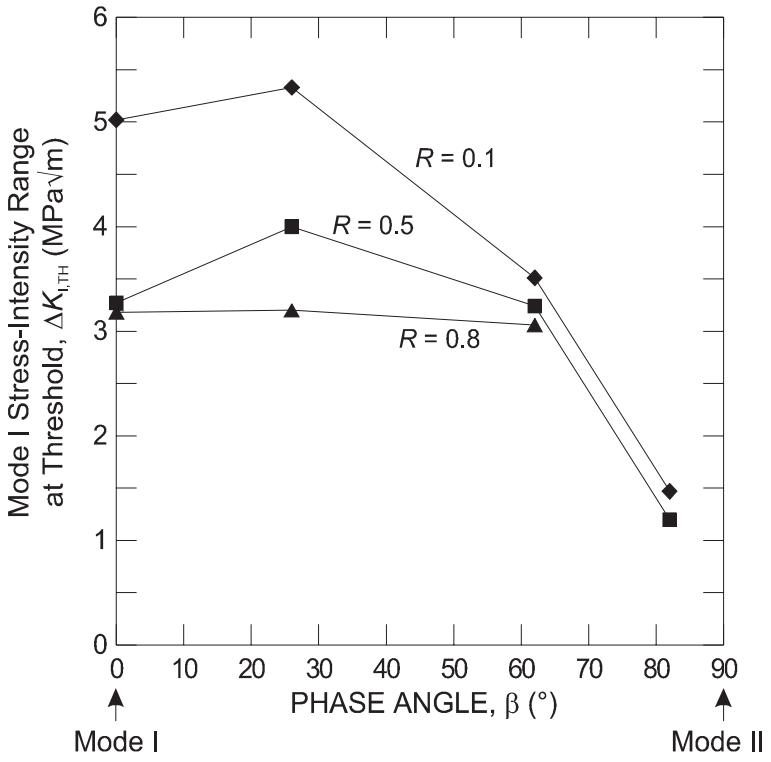

Fig. 5. For the mixed-mode fatigue-crack growth threshold data presented in Fig. 4, the mode I stress-intensity range at threshold, $\Delta K_{I,TH}$, is plotted as a function of the applied phase angle, $\beta = \tan^{-1}(\Delta K_{II}/\Delta K_I)$. $\Delta K_{I,TH}$ is observed to increase slightly as β increases from 0° to 26° ($\Delta K_{II}/\Delta K_I = 0$ and 0.5, respectively) and then decrease for $\beta = 62°$ and 82° ($\Delta K_{II}/\Delta K_I = 1.9$ and 7.1).

While the value of the mode I threshold, $\Delta K_{I,TH}$, is substantially reduced at high phase angles, a conspicuous feature of the mixed-mode threshold envelopes in Fig. 4 is that the value of $\Delta K_{I,TH}$ does not necessarily decrease monotonically with increasing mode-mixity. Its value is actually nominally unchanged (indeed, it is slightly increased) as β is increased from 0° to 26° ($\Delta K_{II}/\Delta K_I = 0$ and 0.5, respectively), for all load ratios investigated. This variation of $\Delta K_{I,TH}$ with phase angle, β, (plotted in Fig. 5) gives rise to the appearance of a "nose" in the threshold envelope. Such a feature in the mixed-mode fatigue-crack growth threshold envelope has not been previously reported in the literature and is contrary to the previous reports of fatigue-crack growth behavior in other material systems [5,8,11,33–35], where the mode I threshold, $\Delta K_{I,TH}$, has been reported to decrease monotonically due to the superposition of shear loading. Furthermore, for the present data, as β is increased to 62° ($\Delta K_{II}/\Delta K_I = 1.9$), the value of $\Delta K_{I,TH}$ does not necessarily decrease substantially relative to its value at $\beta = 0°$, particularly at $R = 0.5$ and 0.8. For $\beta = 82°$ ($\Delta K_{II}/\Delta K_I = 7.1$), however, the mode I threshold stress-intensity range does decrease substantially. As discussed in detail in Part II [36], quantification of crack-tip shielding with respect to the applied mode I stress-intensity range indicates that this insensitivity of $\Delta K_{I,TH}$ to superimposed shear loading can be attributed largely to a shear-induced enhancement of mode I fatigue-crack closure.

3.2. Mixed-mode crack path

Contrary to the previous reports of transient self-similar crack extension during mixed-mode loading in Ti–6Al–4V [5] and other material systems [4,37], such coplanar crack extension was not observed in the

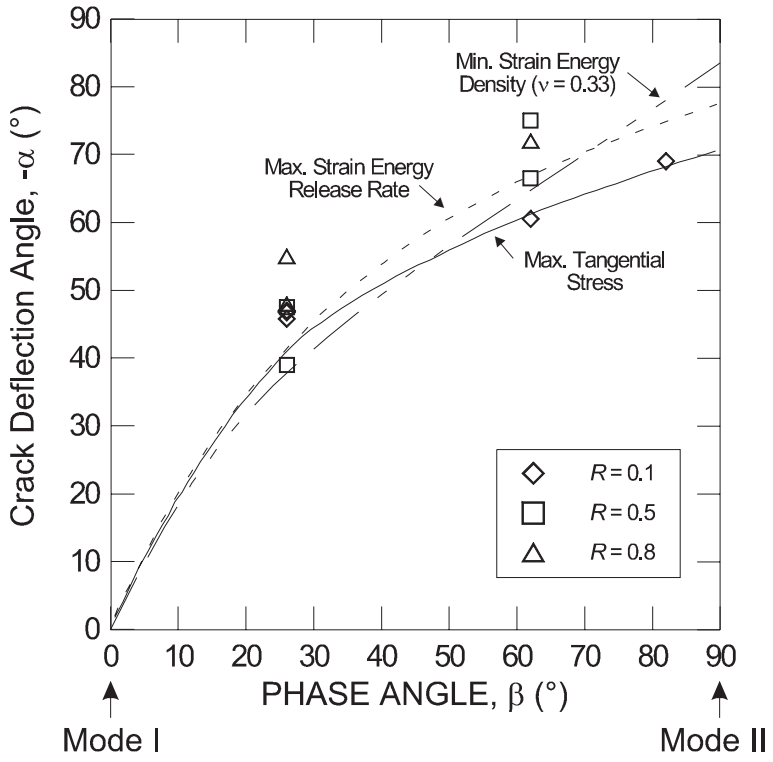

Fig. 6. Measured crack deflection angles, α, are plotted as a function of the applied phase angle, β, for $R = 0.1$, 0.5 and 0.8. These data are compared with the crack deflection angles predicted by the three most prominent theories describing crack propagation under mixed-mode loading conditions: the maximum tangential stress criterion [38], the minimum strain energy density criterion [39], and the maximum strain energy release rate criterion [40].

present study. In all cases, the onset of crack propagation was deflected with respect to the precrack orientation. In Fig. 6, the measured crack deflection angles, α, are plotted as a function of the applied phase angle, β, for $R = 0.1$, 0.5 and 0.8. Note that the length of the deflected cracks used to identify the crack deflection angles were large compared to the microstructural size scales, i.e., ~25 grain diameters. These data are compared with the crack deflection angles predicted by the three most prominent theories describing crack propagation under mixed-mode loading conditions: the maximum tangential stress criterion [38], the minimum strain energy density criterion [39], and the maximum strain energy release rate criterion [40]. Despite the experimental scatter in these data, the present results are generally consistent with any one of these theories, although there is a slight trend of higher crack deflection angles than that predicted by the theory. It has been reported previously for BS4360 50D structural steel [10] that the angle of crack deflection due to an applied mixed-mode loading is not a function of load ratio; the present results do not refute this finding.

3.3. Single-parameter characterization of the mixed-mode threshold

While it is instructive to examine the variation of fatigue-crack growth threshold as a function of mode mixity and load ratio using the threshold envelopes shown in Fig. 4, additional information can be obtained by replotting these same data using a single-parameter characterization of the mixed-mode, crack-driving

force which incorporates both ΔK_I and ΔK_{II}. In Fig. 7a, the mixed-mode fatigue thresholds are presented in terms of the range in strain energy release rate, ΔG: [4]

$$\Delta G_{TH} = (\Delta K_{I,TH}^2 + \Delta K_{II,TH}^2)/E'. \quad (1)$$

Here, $\Delta K_{I,TH}$ and $\Delta K_{II,TH}$ are values of these parameters applied to the precrack tip, $E' = E$ (the elastic modulus) for plane stress, and $E' = E/(1 - \nu^2)$ for plane strain (ν is Poisson's ratio). Alternatively, the results can be plotted in terms of an equivalent stress-intensity range, ΔK_{eq} (Fig. 7b), where the equivalent (mixed-mode) stress-intensity threshold is given by

$$\Delta K_{eq,TH} = (\Delta G_{TH} E')^{1/2}. \quad (2)$$

Using this single-parameter characterization of the fatique-crack growth resistance (Fig. 7), it is apparent that the crack-growth threshold, ΔG_{TH} or $\Delta K_{eq,TH}$, increases monotonically with phase angle, β, for each load ratio investigated. For the highest phase angles investigated ($\beta = 82°$ for $R = 0.1$ and 0.5 and $\beta = 62°$ for $R = 0.8$), ΔG_{TH} is 4.4, 7.0 and 4.1 times the mode I threshold value, respectively, for $R = 0.1$, 0.5 and 0.8. From the perspective of high-cycle fatigue in turbine engine components, the results presented in Fig. 7 indicate that for bimodal Ti–6Al–4V, the mode I ΔG_{TH} fatigue threshold (measured at the appropriate load ratio) represents the worst-case condition for all phase angles measured. Thus, the presence of mixed-mode loading does not preclude the application of a threshold-based design methodology. In fact, a conservative estimate of the mixed-mode threshold can be attained simply by expressing the pure mode I threshold in terms of ΔG. Alternatively, in terms of stress intensities, the lower-bound, mixed-mode threshold condition can be stated as the equivalent stress-intensity range equal to the mode I threshold ΔK measured under pure mode I loading conditions, i.e., $\Delta K_{eq,TH} = \Delta K_{I,TH}$ at $\beta = 0°$. Other examples of the crack-growth resistance increasing with increasing mode-mixity have been reported for monotonic fracture at interfaces [41,42], cyclic-loading induced delamination of Cu/Sn–Pb solder joints [43], and the fatigue of dual-phase steels [11].

3.4. Influence of load ratio

Although the influence of load ratio has been noted above with reference to the mixed-mode threshold envelopes shown in Fig. 4, the relationship between the mixed-mode threshold and R for each phase angle investigated can be more clearly observed in Fig. 8, where ΔG_{TH} is plotted as a function of R for phase angles of $\beta = 0°$, 26°, 62° and 82° ($\Delta K_{II}/\Delta K_I = 0$, 0.5, 1.9 and 7.1, respectively). For each value of β, the fatigue-crack growth threshold decreases as load ratio increases. For the case of mode I loading, a transition is observed between a region where ΔG_{TH} is relatively strongly dependent on load ratio ($R < 0.5$) and a region of significantly reduced load ratio dependence ($R > 0.5$); this behavior is consistent with the model developed by Schmidt and Paris [44] to describe the variation of the mode I fatigue threshold with load ratio. On the assumption that the stress intensity for crack closure, K_{cl}, and the effective (near-tip) threshold stress-intensity range, $\Delta K_{eff,TH}$, are both independent of R, this model predicts that the $\Delta K_{I,TH}$ threshold should be constant with R above a critical load ratio where K_{min} first exceeds K_{cl} (such that closure effects are minimal). Indeed, this relationship between the mode I fatigue-crack growth threshold and R has been documented previously for the same bimodal Ti–6Al–4V investigated in this study [14,24,25], and these findings were consistent with the current results.

[4] It should be noted that ΔG defined this way is not exactly equal to $G_{max} - G_{min}$, where G_{max} and G_{min} are, respectively, the values of G determined at the maximum and minimum loads of the fatigue cycle.

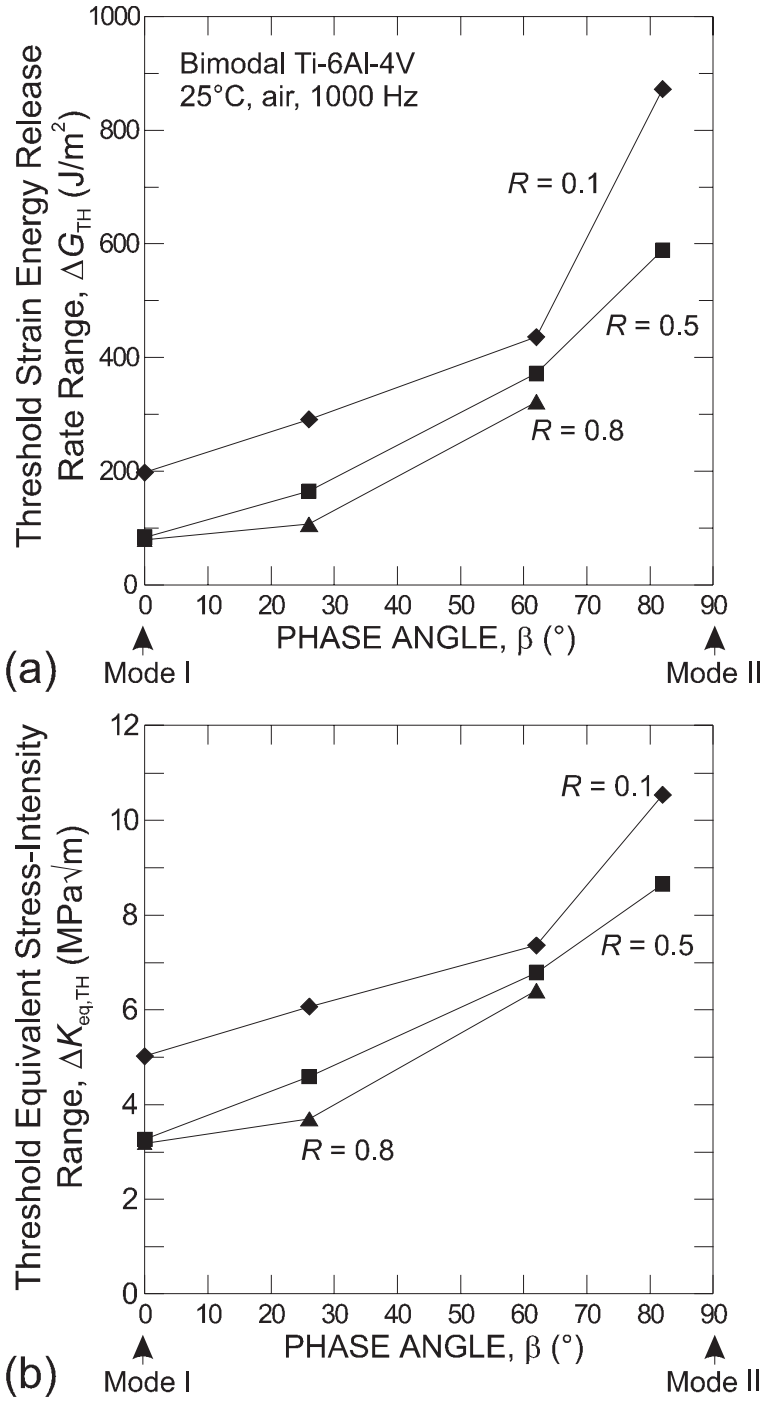

Fig. 7. Mixed-mode fatigue-crack growth thresholds in bimodal Ti–6Al–4V are plotted in terms of (a) the range in strain energy release rate at threshold, ΔG_{TH}, and (b) the equivalent stress-intensity range, $\Delta K_{eq,TH} = (\Delta G_{TH} E')^{1/2}$, as a function of the applied phase angle, $\beta = \tan^{-1}(\Delta K_{II}/\Delta K_I)$, for load ratios of 0.1, 0.5 and 0.8. ΔG_{TH} is observed to increase substantially with β.

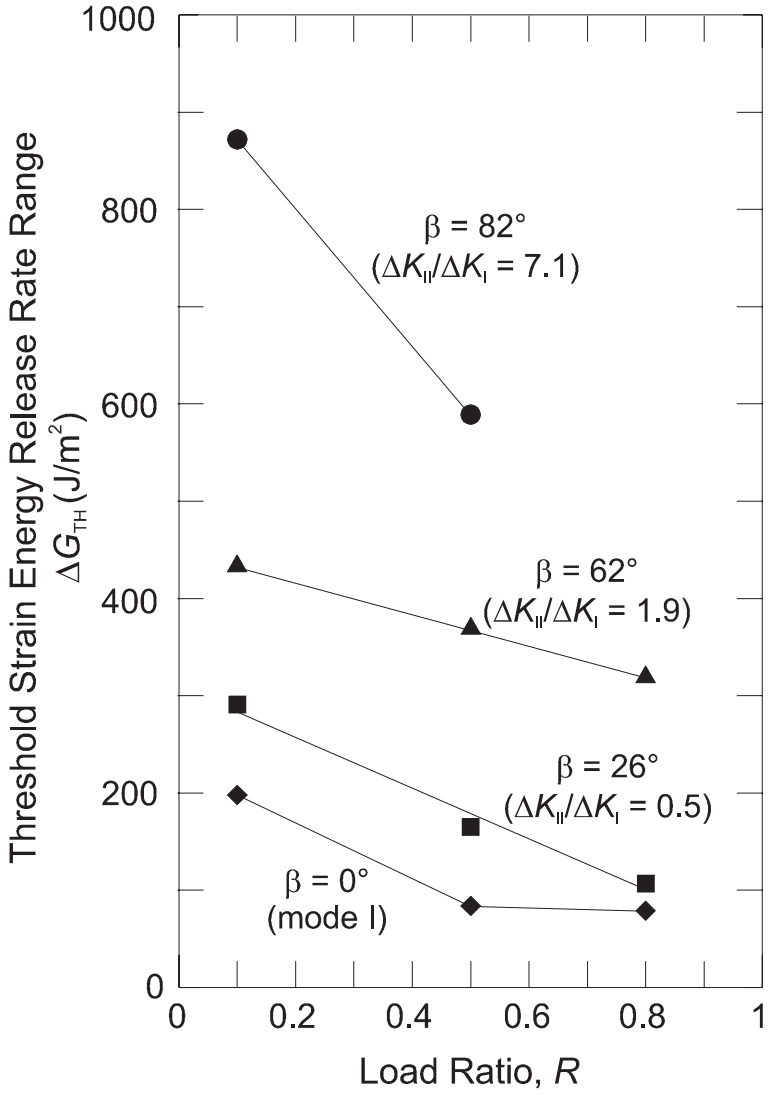

Fig. 8. The threshold range in strain energy release rate, ΔG_{TH}, is plotted as a function of load ratio, R, for $\beta = 0°$, 26°, 62° and 82° ($\Delta K_{II}/\Delta K_I = 0$, 0.5, 1.9 and 7.1, respectively). For each value of β, the fatigue-crack growth threshold decreases as load ratio increases.

For the mixed-mode loading conditions investigated ($\beta = 26°$, 62°, and 82°), the relationship between ΔG_{TH} and R is distinctly different from the behavior exhibited for mode I loading ($\beta = 0°$). Specifically, the fatigue threshold is observed to decrease at a nearly constant rate with increasing load ratio, i.e., there is no transition between regimes of relatively strong and weak load ratio dependence. Quantification of mixed-mode crack-tip shielding (reported in Part II [36]) suggests that the absence of such a transition may be attributed to enhanced crack-tip shielding under mixed-mode loading (where shielding is not fully suppressed even at $R = 0.8$). A constant rate of decrease of mixed-mode fatigue-crack growth thresholds with increasing R has previously been observed in BS4360 50D structural steel by Tong et al. [10]. However, in that study, the rate of decrease in the threshold was reported to be the same for all phase angles investigated

and equal to the initial slope of the mode I threshold versus R data. Here, the slope of ΔG_{TH} versus R for $\beta = 26°$ and 62° are similar to that of the strongly R-dependent regime of the mode I threshold data, but each of these slopes is indeed slightly different.

For $\beta = 82°$ ($\Delta K_{II}/\Delta K_I = 7.1$), it appears that the threshold is much more strongly dependent on load ratio than for any other phase angle investigated. This finding must be questioned, however, because for fatigue loading with $\beta = 82°$ and $R = 0.5$, crack extension was observed to occur by the formation of a branch crack which deflected off the precrack wake approximately 275 μm behind the crack tip (this result was reproducible in more than one sample). At this point in the crack wake, $\Delta K_{II}/\Delta K_I$ is not equal to 7.1. Hence, the fatigue-crack growth threshold reported here for $\beta = 82°$, $R = 0.5$ should be viewed as a conservative estimate and the dependence of the threshold on load ratio for $\beta = 82°$ may not be as strong as suggested in Fig. 8.

3.5. Short-crack fatigue thresholds for mixed-mode loading conditions

Mixed-mode fatigue-crack thresholds for short cracks in bimodal Ti–6Al–4V are compared with the threshold data for large cracks at $R = 0.1$ and 0.8 in Fig. 9. Short-crack threshold measurements were performed at $R = 0.1$ and 1000 Hz cyclic loading frequency in ambient temperature air. Threshold data for applied phase angles, $\beta = \tan^{-1}(\Delta K_{II}/\Delta K_I)$, of 26°, 62° and 82° ($\Delta K_{II}/\Delta K_I = 0.5$, 1.9 and 7.1, respectively) are presented in terms of the threshold mode II stress-intensity range, $\Delta K_{II,TH}$, as a function of the corresponding mode I value, $\Delta K_{I,TH}$, in Fig. 9a. In Fig. 9b, the mixed-mode threshold, in terms of ΔG_{TH}, is plotted as a function of the phase angle, β.

For each phase angle investigated, the short-crack fatigue threshold is considerably lower than that of the corresponding large crack at $R = 0.1$. This is particularly clear under shear-dominant loading conditions at $\beta = 62°$ and 82°. The reduction in the threshold for fatigue-crack growth with cracks of restricted wake is believed to arise from the limited extent of crack-tip shielding that can develop for short fatigue cracks. Also, the dependence on mode-mixity of the ΔG_{TH} threshold for the short fatigue cracks is markedly reduced compared to the ΔG_{TH} dependence on β for large cracks. Whereas, the large-crack ΔG_{TH} threshold increases by as much as a factor of 7 with superimposed shear, the short-crack threshold at $R = 0.1$ increases by only a factor of ~2.5. If it is assumed that the primary difference between the large and short fatigue cracks is the magnitude of crack-tip shielding [15], the present results suggest that such shielding contributes significantly to the magnitude of the large-crack mixed-mode thresholds, and is largely responsible for the elevation in the ΔG_{TH} threshold as β is increased. Moreover, the mixed-mode fatigue-crack growth resistance may be even worse for incipient surface cracks that are of dimensions equivalent or less than the microstructural size scales. For such microstructurally-small cracks, in addition to a biased sampling of the microstructure, the magnitude of crack-tip shielding would likely be even less than that which exists for the short fatigue cracks investigated here (where crack lengths are ~10 times the average grain size). This point is discussed in more detail in Section 3.6.

It is noted that, as no measurement of the pure mode I, short-crack threshold was made, the large-crack value of ΔG_{TH} at $R = 0.8$ is used as an estimate of this data point in Fig. 9b for purposes of illustrating the variation of ΔG_{TH} with β for short fatigue cracks at $R = 0.1$. For mode I fatigue-crack growth in the bimodal Ti–6Al–4V of interest here, it has been shown that (global) crack-tip shielding (i.e., crack closure) is completely suppressed at $R = 0.8$ [45]. Thus, it is expected that the large-crack threshold measured at $R = 0.8$ would be comparable to a threshold measured from a short fatigue crack at $R = 0.1$, where closure is now largely suppressed by the limited crack wake length. Although, in general, mean stress may influence the fatigue-crack growth threshold independent of crack closure [46–48], this effect is not significant in the present material for load ratios between that necessary to fully suppress closure ($R = 0.5$) and $R = 0.8$; specifically, only a 0.3 MPa $\sqrt{m}$ reduction in $\Delta K_{I,TH}$ is observed between these R ratios [45].

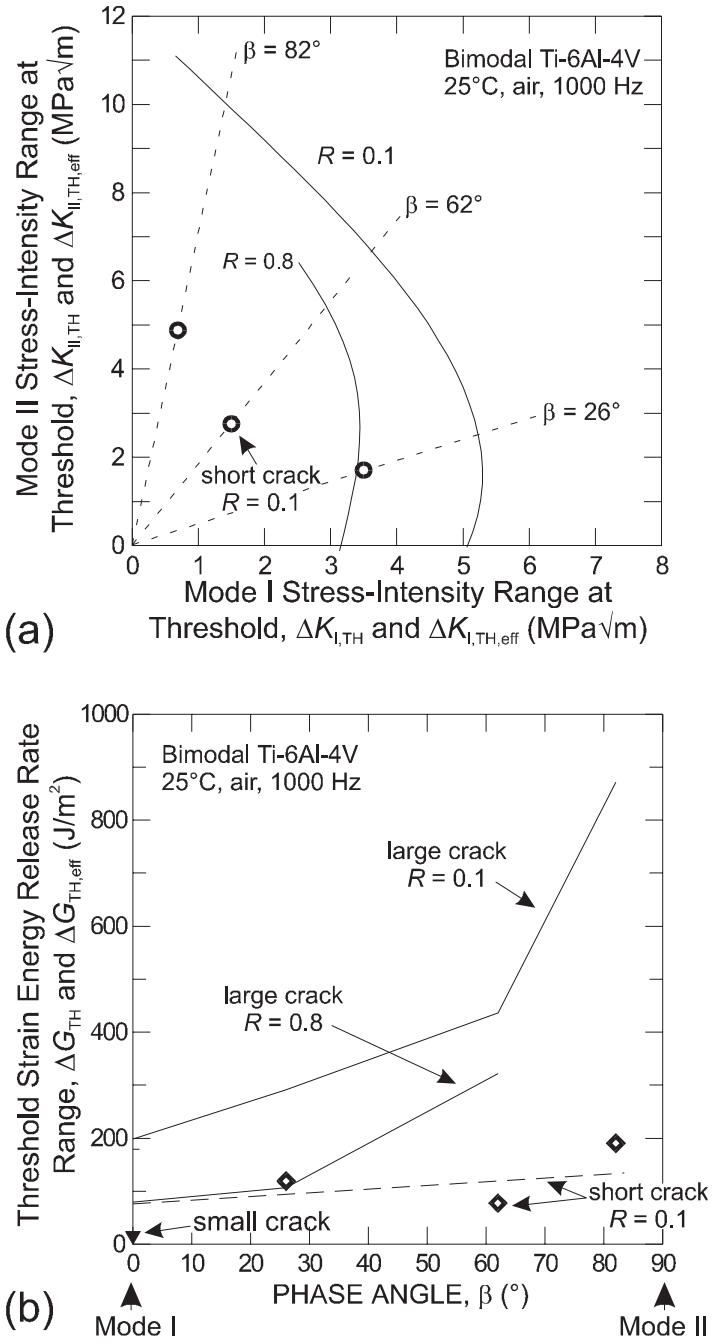

Fig. 9. Mixed-mode fatigue-crack growth thresholds for short cracks in bimodal Ti–6Al–4V ($R = 0.1$, 1000 Hz cyclic loading frequency) are compared with threshold data for large fatigue cracks at $R = 0.1$ and 0.8. Threshold data are presented both in terms of (a) the threshold mode II stress-intensity range, $\Delta K_{II,TH}$, as a function of the corresponding mode I value, $\Delta K_{I,TH}$, and (b) the threshold range in strain energy release rate, ΔG_{TH}, as a function of the applied phase angle, $\beta = \tan^{-1}(\Delta K_{II}/\Delta K_I)$. Also shown in (b) is an estimate of the mode I fatigue-crack growth threshold for a microstructurally small crack [49].

3.6. Fatigue-crack growth thresholds in the presence of microstructurally small cracks

While consideration has already been given to the manner in which the mixed-mode fatigue-crack growth threshold varies with the applied ratio $\Delta K_{II}/\Delta K_I$ in the absence of crack-tip shielding, it is important to remember that fatigue-crack growth resistance can also be significantly altered when the crack front samples a limited number of microstructural entities. In Fig. 9, a mode I fatigue-crack growth threshold ($R = 0.1$) is presented for a naturally initiated small crack in bimodal Ti–6Al–4V, which is on the order of the grain size of this material (~20 μm). This data point, measured by Peters and Ritchie [49], indicates that fatigue-crack growth can occur at applied driving forces as low as $\Delta K_{I,TH} = 1$ MPa $\sqrt{m}$ ($\Delta G_{TH} = 9.5$ J/m^2). This microstructurally small-crack threshold illustrates the marked influence which the biased microstructural sampling can have on the fatigue-crack growth threshold. Such behavior has been well documented for mode I fatigue loading [16–22], but has never been examined in terms of mixed-mode loading. Comparison of this small-crack threshold with a crack-tip shielding free, large-crack threshold ($R = 0.8$, $\Delta K_{I,TH} = 3.2$ MPa $\sqrt{m}$ and $\Delta G_{TH} = 79$ J/m^2) subjected to an equivalent phase angle ($\beta = 0°$) indicates that such restricted sampling of the microstructure can reduce the fatigue-crack growth threshold by factors of ~3 and 8, respectively, in terms of $\Delta K_{I,TH}$ and ΔG_{TH}. It is also interesting to note the full range in fatigue-crack growth threshold that can be exhibited in bimodal Ti–6Al–4V due to variations in applied phase angle, crack size, and microstructural sampling. For $R = 0.1$ and $\beta = 82°$ ($\Delta K_{II}/\Delta K_I = 7.1$), the measured large-crack threshold, $\Delta G_{TH} = 872$ J/m^2, is a *factor 90 times higher than this mode I small crack threshold*. [5] Clearly, further work is needed to determine the small-crack thresholds under mixed-mode loading conditions in order to complete the understanding of mixed-mode fatigue-crack growth resistance.

4. Conclusions

Based on a study of the high-cycle, fatigue-crack growth threshold for both large (>4 mm) and short (~200 μm) cracks under combined mode I and mode II loading (mode-mixities varying from $\Delta K_{II}/\Delta K_I = 0$ to ~7; phase angles from 0° to 82°) in a Ti–6Al–4V turbine blade alloy with a bimodal (STOA) microstructure, tested in room temperature air at a loading frequency of 1000 Hz (sine wave), the following conclusions are made:

(1) Although the large-crack, mode I fatigue threshold stress-intensity range, $\Delta K_{I,TH}$, is found to decrease for sufficiently high mode-mixity ($\Delta K_{II}/\Delta K_I$), more appropriate quantification of the crack driving force in terms of the range in strain-energy release rate reveals that the mixed-mode threshold, ΔG_{TH}, actually increases; indeed, for an increase in mode-mixity from $\Delta K_{II}/\Delta K_I = 0$ to ~7, a sevenfold increase in ΔG_{TH} has been observed. Thus, for "continuum-sized" cracks (i.e., large compared to microstructural dimensions) in this alloy, the pure mode I threshold, defined in terms of ΔG_{TH}, may be used as a conservative, lower-bound estimate of the mixed-mode fatigue-crack growth threshold.

(2) Measurements of short-crack fatigue thresholds, where the wake shielding zone is restricted to ~200 μm, suggest that this significant increase in the large-crack, mixed-mode ΔG_{TH} threshold with increasing mode-mixity is primarily due to a shear-induced enhancement of crack-tip shielding. For the short fatigue cracks, where such shielding is minimal, the measured ΔG_{TH} thresholds are significantly lower (relative to the large-crack threshold) for all values of $\Delta K_{II}/\Delta K_I$ investigated. Moreover, the increase in ΔG_{TH} with increasing mode-mixity is markedly reduced.

[5] When the thresholds are compared in terms of an equivalent stress-intensity range, $\Delta K_{eq,TH}$, the mixed-mode large-crack threshold at $R = 0.1$ and $\beta = 82°$ is still a factor of ~9.5 higher than the mode I small-crack threshold ($\Delta K_{eq,TH} = 10.5$ and 1.1 MPa $\sqrt{m}$, respectively).

(3) For both mode I and mixed-mode loading conditions, the threshold for fatigue-crack growth decreases with increasing positive load ratio ($R = 0.1$–0.8). For mode I loading, at a critical load ratio ($R_{cr} \sim 0.5$) above which crack closure effects are minimal (i.e., $K_{min} > K_{cl}$), a transition is observed between regimes of relatively strong load-ratio dependence (for $R < R_{cr}$) and relatively weak load-ratio dependence (for $R > R_{cr}$). Conversely, for mixed-mode loading conditions, no such transition is observed; the rate of decrease in mixed-mode ΔG_{TH} threshold with increasing R is relatively constant over the range of $R = 0.1$–0.8. Such behavior is reasoned to result from an increase in crack-tip shielding with increasing mode-mixity due to shear-induced crack-surface interference.

Acknowledgements

This work was supported by the US Air Force Office of Scientific Research under Grant No. F49620-96-1-0478 under the auspices of the Multidisciplinary University Research Initiative on *High Cycle Fatigue* to the University of California.

Appendix A. Distinction between large, short and small cracks

A key component of the present work is a comparison of the mixed-mode crack-growth behavior for fatigue cracks of varying dimension, which are classified here as *large*, *short* and *small* cracks. For the sake of clarity, the salient differences between such cracks are briefly reviewed here. Large fatigue cracks (Fig. 10a) have fracture surface dimensions that are large compared to the scale of the microstructure in both directions. They therefore generally have a fully developed [6] crack-tip shielding zone and can "sample" the microstructure in a statistical (continuum) manner [21]. With respect to large cracks, small cracks are generally described as being comparable in size to [20]:

(i) microstructural dimensions, where biased statistical sampling of the microstructure can lead to accelerated crack advance along "weak" paths, i.e., microstrucutral features oriented for easy crack growth (a continuum limitation);

(ii) the extent of local inelasticity *ahead* of the crack tip, where the assumption of small-scale yielding implicit in the use of the stress intensity, K, is not strictly valid (a linear-elastic fracture mechanics limitation);

(iii) the extent of crack-tip shielding (e.g., crack closure) *behind* the crack tip, where the reduced role of shielding leads to a higher local driving force than the corresponding large crack at the same applied K level (a similitude limitation).

However, a further important distinction can be made, namely that of a short vs. small crack, as schematically shown in Fig. 10. This distinction alludes not simply to physical size but the extent to which a fatigue crack is subjected to the first and third factors listed above. Short fatigue cracks (Fig. 10b) are physically short in only one dimension, a condition that is often realized experimentally by machining away the wake of a large crack. This type of fatigue flaw experiences limited crack-tip shielding due to its reduced length [15], yet still samples the microstructure as a continuum because of its extensive crack front. In contrast, small fatigue cracks (Fig. 10c) are small and comparable to the microstructural size scale in all dimensions, as typified by the small, semi-elliptical surface flaw [19,20,22]. With such cracks, crack-tip

[6] For mixed-mode loading conditions, the shearing of the fracture surfaces with respect to one another can produce crack-wake contact via sliding interference over dimensions which are much larger than for mode I loading, perhaps over the entire wake of a large fatigue crack [28,50]. Thus, the notion of a "fully developed" shielding zone is somewhat unclear for mixed-mode loading conditions. At the least, one would expect the equilibrium shielding-zone length to be a function of the applied ratio of shear to tension.

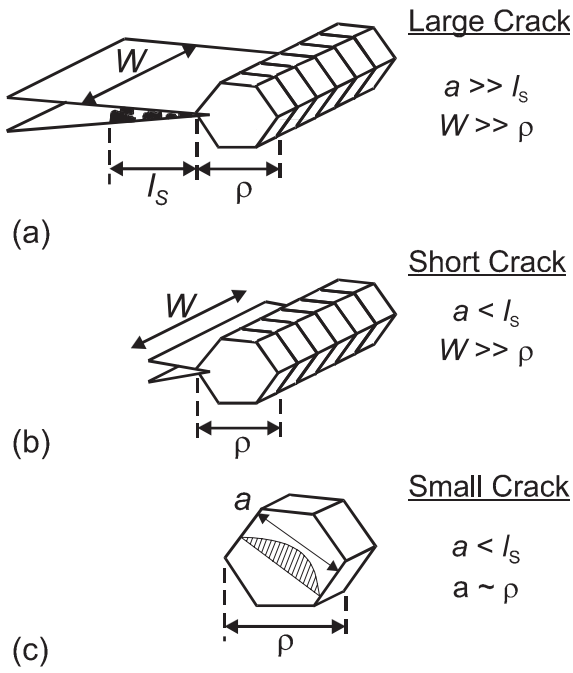

Fig. 10. These schematic illustrations highlight the key distinctions between large, short and small fatigue cracks. Large cracks (a) have length, a, and width, W, which are large both with respect to the equilibrium shielding-zone length, l_s (indicated here as a region of debris in the crack wake which produces crack closure), and the characteristic microstructural size scale, ρ, e.g., the grain size. In contrast to this, short fatigue cracks (b) are characterized by $a < l_s$, but $W \gg \rho$. The reduced crack-wake length results in a lower level of crack-tip shielding. For small cracks (c), the fracture surface is reduced in both dimensions, with a (and W) being small with respect to both l_s and ρ. The fact that $a \sim \rho$ implies that the crack front samples only a few microstructural entities, leading to a biased sampling of the microstructure.

shielding is significantly reduced [17,21], and since the crack front samples only few microstructural entities, this allows a biased sampling of microstructurally weak paths [18]. Because of this restriction in shielding and the biased microstructural sampling, fatigue-crack growth resistance in the presence of small cracks tends to be lowest.

Appendix B. Error analysis

The attainment of the desired phase angle, $\beta = \tan^{-1}(\Delta K_{II}/\Delta K_I)$, using the asymmetric four-point bend loading geometry (Fig. 2) [26], requires that the crack be offset from the load line of the mechanical testing frame by a specific amount. Errors in the value of this offset, s, can lead to significant errors in β and ΔK_I. This is particularly true when trying to achieve strongly shear-dominant loading conditions, as the value of $\Delta K_{II}/\Delta K_I$ approaches infinity as $s \to 0$. As shown in Fig. 2, for the asymmetric four-point bend test, the bending moment, M_z, varies linearly between the inner loading points, while the shear force, F_{xy}, is constant in this region. As a result, uncertainty in s leads to uncertainty in ΔK_I and, hence, in the phase angle; ΔK_{II} is unaffected.

For the mixed-mode fatigue-crack growth threshold measurements made in the present study, the error in s was quantified by comparing the expected position of the crack with respect to the load line (based on a positioning of the sample using a micrometer) and to the true value of s (determined by measuring the

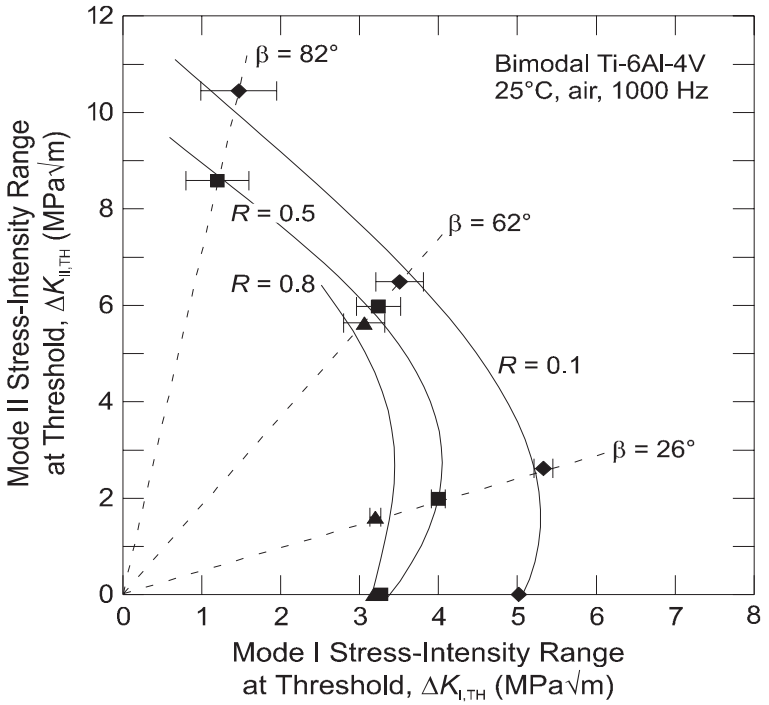

Fig. 11. The root mean squared error in the crack offset from the load line, s, was determined to be 0.081 mm. The uncertainty in $\Delta K_{I,TH}$, which arises because of this uncertainty in s, is indicated in the mixed-mode fatigue-crack growth threshold envelopes by error bars. These error bars span the range in $\Delta K_{I,TH}$ corresponding to the desired value of $s \pm 0.081$ mm.

Table 2
Uncertainty in applied phase angle, β, for bimodal Ti–6Al–4V

Prescribed phase angle β (deg)	Actual range in β (deg)		
	$R = 0.1$	$R = 0.5$	$R = 0.8$
0	0	0	0
26	25.6–26.6	25.8–26.9	26.1–27.1
62	59.5–63.6	59.5–63.6	59.5–63.6
82	79.4–84.6	79.4–84.7	–

distance from the load line to the crack tip using an optical telescope). The root mean squared error in s was determined to be only 0.081 mm. The resultant uncertainty in the mixed-mode fatigue-crack growth threshold data for bimodal Ti–6Al–4V is presented in Fig. 11, where error bars indicate the range in $\Delta K_{I,TH}$ corresponding to ± 0.081 mm with respect to the desired value of s. In accordance with the discussion above, the uncertainty in $\Delta K_{I,TH}$ is larger for the higher phase angle loading conditions. The uncertainty in β is presented in Table 2 in terms of ranges in β (corresponding to the ranges in $\Delta K_{I,TH}$ shown in Fig. 11).

References

[1] Cowles BA. High cycle fatigue in aircraft gas turbines – an industry perspective. Int J Fract 1996;80:147–63.
[2] Nicholas T, Zuiker JR. On the use of the Goodman diagram for high cycle fatigue design. Int J Fract 1996;80:219–35.

[3] Waterhouse RB, Lindley TC, editors. Fretting Fatigue, European Structural Integrity Society Publication No. 18, London: Mechanical Engineering Publications, 1994.
[4] Gao H, Brown MW, Miller KJ. Mixed-mode fatigue thresholds. Fatigue Engng Mater Struct 1982;5:1–17.
[5] Gao H, Alagok N, Brown MW, Miller KJ. Growth of fatigue cracks under combined mode I and mode II loads. In: Miller KJ, Brown MW, editors. Multiaxial fatigue, ASTM STP 853. ASTM, Philadelphia, PA, 1985. p. 184–202.
[6] Pustejovsky MA. Fatigue crack propagation in titanium under general in-plane loading – I. Experiments. Engng Fract Mech 1979;11:9–15.
[7] Pustejovsky MA. Fatigue crack propagation in titanium under general in-plane loading – II. Analysis. Engng Fract Mech 1979;11:17–31.
[8] Tanaka K. Fatigue crack propagation from a crack inclined to the cyclic tensile axis. Engng Fract Mech 1974;6:493–507.
[9] Tong J, Yates JR, Brown MW. The influence of precracking techniques on fatigue crack growth thresholds under mixed mode I/II loading conditions. Fatigue Fract Engng Mater Struct 1994;17:1261–9.
[10] Tong J, Yates JR, Brown MW. The significance of mean stress on the fatigue crack growth threshold for mixed mode I + II loading. Fatigue Fract Engng Mater Struct 1994;17:829–38.
[11] Zheng YS, Wang ZG, Ai SH. Mixed-mode I and II fatigue threshold and crack closure in dual-phase steels. Metall Mater Trans A 1994;25A:1713–23.
[12] Iida S, Kobayashi AS. Crack-propagation rate in 7075-T6 plates under cyclic tensile and transverse shear loading. J Bas Engng 1969;91:764–9.
[13] John R, DeLuca D, Nicholas T, Porter J. Near-threshold crack growth behavior of a single crystal Ni-base superalloy subjected to mixed mode loading. In: Miller KJ, McDowell DL, editors. Mixed-mode crack behavior, ASTM STP 1359. ASTM, West Conshohocken, PA, 1999. p. 312.
[14] Ritchie RO, Davidson DL, Boyce BL, Campbell JP, Roder O. High-cycle fatigue of Ti–6Al–4V. Fatigue Fract Engng Mater Struct 1999;22:621–31.
[15] Ritchie RO, Yu W. Short crack effects in fatigue: a consequence of crack tip shielding. In: Ritchie RO, Lankford J, editors. Small fatigue cracks, TMS-AIME, Warrendale, PA, 1986. p. 167–189.
[16] Campbell JP, Kruzic JJ, Lillibridge S, Venkateswara Rao KT, Ritchie RO. On the growth of small fatigue cracks in γ-based titanium aluminides. Scripta Mater 1997;37:707–12.
[17] Campbell JP, Venkateswara Rao KT, Ritchie RO. The effect of microstructure on fracture toughness and fatigue crack growth behavior in γ-titanium aluminide based intermetallics. Metall Mater Trans A 1999;30A:563–77.
[18] Kruzic JJ, Campbell JP, Ritchie RO. On the fatigue behavior of γ-based titanium aluminides: role of small cracks. Acta Mater 1999;47:801–16.
[19] Davidson DL, Campbell JB, Page RA. The initiation and growth of fatigue cracks in a titanium aluminide alloy. Metall Trans A 1991;22A:377–91.
[20] Ritchie RO, Lankford J. Small fatigue cracks: a statement of the problem and potential solutions. Mater Sci Engng 1986;A84:11–6.
[21] Suresh S, Ritchie RO. Propagation of short fatigue cracks. Int Metals Rev 1984;29:445–76.
[22] Venkateswara Rao KT, Yu W, Ritchie RO. On the behavior of small fatigue cracks in commercial aluminum-lithium alloys. Fract Engng Mech 1988;31:623–35.
[23] Eylon D. Summary of the available information on the processing of the Ti–6Al–4V HCF/LCF program plates, University of Dayton Report, 1998.
[24] Boyce BL. MS Thesis, University of California at Berkeley, 1998.
[25] He MY, Cao HC, Evans AG. Mixed-mode fracture: the four-point shear specimen. Acta Metall Mater 1990;38:839–46.
[26] He MY, Hutchinson JW. Asymmetric four-point crack specimen. J Appl Mech 2000;67:207–9.
[27] Suresh S, Shih CF, Morrone A, O'Dowd NP. Mixed-mode fracture toughness of ceramic materials. J Am Ceram Soc 1990;73:1257–67.
[28] Nayeb-Hashemi H, McClintock FA, Ritchie RO. Effects of friction and high torque on fatigue crack propagation in mode III. Metall Trans A 1982;13A:2197–204.
[29] Smith MC, Smith RA. Toward an understanding of mode II fatigue crack growth. In: Fong JT, Fields RJ, editors. Basic questions in fatigue, vol. I, ASTM STP 924, ASTM, Philadelphia, PA, 1988. p. 260–280.
[30] Tong J, Yates JR, Brown MW. A model for sliding mode crack closure. I: theory for pure mode II loading. Fract Engng Mech 1995;52:599–611.
[31] Tong J, Yates JR, Brown MW. A model for sliding mode crack closure. II: mixed mode I and II loading and application. Engng Fract Mech 1995;52:613–23.
[32] Morgan JM, Milligan WW. A 1 kHz servohydraulic fatigue testing system. In: Soboyejo WO, Srivatsan TS, editors. High cycle fatigue of structural materials, TMS, Warrendale, PA, 1997. p. 305–12.
[33] Pook LP. An observation on mode II fatigue crack growth threshold behavior. Int J Fract 1977;13:867–9.
[34] Tong J, Yates JR, Brown MW. The formation and propagation of mode I branch cracks in mixed mode fatigue failure. Engng Fract Mech 1997;56:213–31.

[35] Liu P, Wang Z. Mixed-mode I and II fatigue threshold and crack deflection angle in SiCp/2024Al composite. Scripta Mater 1996;34:1323–30.
[36] Campbell JP, Ritchie RO. Mixed-mode, high-cycle, fatigue-crack growth thresholds in Ti–6Al–4V: Part II – quantification of crack-tip shielding. Engng Fract Mech 2000;67:229–49.
[37] Otsuka A, Tohgo K, Matsuyama H. Fatigue crack initiation and growth under mixed mode loading in aluminum alloys 2017-T3 and 7075-T6. Engng Fract Mech 1987;28:721–32.
[38] Erdogan F, Sih GC. On the crack extension in plates under plane loading and transverse shear. J Bas Engng 1963;85: 519–25.
[39] Sih GC. Strain energy density factor applied to mixed mode crack problems. Int J Fract 1974;10:305–21.
[40] Cotterell B. On brittle fracture paths. Int J Fract Mech 1965;1:96–103.
[41] Thouless MD. Fracture of a model interface under mixed-mode loading. Acta Metall Mater 1990;38:1135–40.
[42] O'Dowd NP, Stout MG, Shih CF. Fracture toughness of alumina-niobium interfaces: experiments and analyses. Philos Mag A 1992;66:1037–64.
[43] Yao D, Shang JK. Effect of load-mix on fatigue crack growth in 63Sn-37Pb solder joints. Trans ASME J Electron Packag 1997;119:114–8.
[44] Schmidt RA, Paris PC. Threshold for fatigue crack propagation and effects of load ratio and frequency. Progress in flaw growth and fracture toughness testing, ASTM STP 536. ASTM, Philidelphia, PA, 1973. p. 79–94.
[45] Ritchie RO, Boyce BL, Campbell JP, Roder O, Thompson AW, Milligan WW. Thresholds for high-cycle fatigue in a turbine engine Ti–6Al–4V alloy. Int J Fatigue 1999;21:653–62.
[46] Boyce BL, Ritchie RO. Effect of load ratio and maximum stress intensity on the fatigue threshold in Ti–6Al–4V, Engng Fract Mech 2000, submitted for publication.
[47] Döker H. Fatigue crack growth threshold: implications, determination and data evaluation. Int J Fatigue 1997;19:S145–9.
[48] Huthmann H, Gossmann O. Verband für Materialforschung und –prüfung. Vortragsveranstaltung des DVM-Arbeitskreises Bruchvorgänge, Deutscher 1981. p. 271–4.
[49] Peters JO, Ritchie RO. Influence of foreign-object damage on crack initiation and early crack growth during high-cycle fatigue of Ti–6Al–4V. Engng Fract Mech 2000;67:193–207.
[50] Tschegg EK. Sliding mode crack closure and mode III fatigue crack growth in mild steel. Acta Metall 1983;31:1323–30.